Emergent Materials (2025) 8:8055–8072
https://doi.org/10.1007/s42247-025-01258-7

ORIGINAL ARTICLE

Synthesis of Fe-Zn-Al Layered double oxide for effective adsorptive removal of trace metal(loid)s: optimisation, isotherms, kinetics and application to real water samples

Ramatsobane Rosy Phogole[1,2] · Philani Perfect Mpungose[3] · Luthando Nyaba[1,2] · Mthokozisi Mnguni[1,2] · Philiswa Nosizo Nomngongo[1,2]

Received: 26 May 2025 / Accepted: 18 September 2025 / Published online: 9 October 2025

Abstract
The layered double oxides (LDO) have gained attention as sorbets for decontaminating metal (loid)s for wastewater treatment. These materials are prepared from LDH by thermal treatment, whereby LDHs are calcined to remove interlayer anions. This study synthesised Fe-Zn-Al-LDO from Fe-Zn-Al LDH via thermal treatment to decontaminate As, Cd, and Pb in wastewater. The synthesised Fe-Zn-Al LDO was characterised using various analytical characterisation techniques. The transmittance electron microscopy (TEM) results showed that Fe-Zn-Al-LDO had spherically shaped particles with an average size of 12.1 ± 1.7 nm. The Brunauer–Emmett–Teller (BET) surface area and pore volume of the Fe-Zn-Al LDO material were 88.1 m^2/g and 0.35 cm^3/g. Under optimum conditions, Fe-Zn-Al LDO adsorbent had an excellent adsorption efficiency for As, Cd and Pb, with maximum adsorption capacities of 233 mg/g, 204 mg/g and 256 mg/g, respectively. The kinetics and isotherm studies revealed that the adsorption process of the analytes onto Fe-Zn-Al LDO adsorbent followed pseudo-second order and Freundlich isotherm models. The Fe-Zn-Al LDO materials were utilised as an adsorbent to remove As, Cd and Pb from groundwater and surface water spiked with 1000 µg/L of analytes, and the results showed that the adsorbent reduced the concentrations of these analytes to levels below the acceptable contamination levels. With the systematic study of adsorptive removal of trace metal(loid)s using Fe-Zn-Al LDO adsorbent, a promising adsorption technology was developed to address pollution of drinking water sources.

Keywords Fe-Zn-Al LDO nanoparticles · Thermal treatment · Equilibrium studies · Environmental water samples · Potentially toxic elements

1 Introduction

Surface water and groundwater are the primary drinking water sources in many rural areas of South Africa, and these water resources are critical for water supply development [1, 2]. A recent study conducted in Eastern Cape Province, South Africa, revealed that surface water and groundwater account for more than 50% total water supply [3]. Another study on surface water and groundwater sources in the Eastern Cape Province revealed that the concentrations of heavy metals such as Cd(II) and Pb(II) were higher than the World Health Organisation (WHO) and South African standards. African National Standard (SANS 241) recommended permissible limits for drinking water [4]. Increasing human activities have resulted in drastic pollution of water systems by heavy metal(loid)s. Surface water and groundwater

✉ Philiswa Nosizo Nomngongo
pnnomngongo@uj.ac.za

1 Department of Chemical Sciences, University of Johannesburg, Doornfontein Campus, P.O. Box 17011, Doornfontein 2028, South Africa

2 Department of Science and Innovation, National Research Foundation South African Research Chair Initiative (DSI-NRF SARChI) in Nanotechnology for Water, University of Johannesburg, Doornfontein 2028, South Africa

3 Department of Chemistry, Cape Peninsula University of Technology, Cape Town 2000, South Africa

pollution in rural areas emanates from the agricultural sector, geogenic bedrock, steel and metal processing, and improper waste disposal [5]. Arsenic, Cd, and Pb occur naturally in the Earth's crust, and owing to their carcinogenic effects and toxicity, they are considered the most hazardous substances [6, 7]. The occurrence of these contaminants in surface water and groundwater sources may cause serious threats to public health and environmental safety [8]. Previous studies have reported that excessive intake of water containing As(III), Cd(II), and Pb(II) could cause other acute and chronic health effects, such as cardiovascular diseases, kidney damage, high blood pressure and neurological disorders, among others [7, 9, 10]. Furthermore, the presence of As(III), Cd(II), and Pb(II) species in drinking water sources degrades water quality, thus threatening water security in rural communities [11, 12]. Therefore, it is important to develop methodologies for the removal/reduction of As(III), Cd(II), and Pb(II) species concentrations in drinking water sources to levels below the permissible limits.

Various methods, including lime coagulation, chemical precipitation, reverse osmosis, ion exchange, solvent extraction, and adsorptive removal, are currently employed to remove trace metal(loid)s from our water systems [13, 14]. However, this study will focus on adsorption because it is cost-effective, easy to operate, flexible, and exhibits high removal performance [15].

The removal efficiency of an adsorption process largely depends on the interaction between the adsorption sites on the material and the target analytes. The number of adsorption sites and their effectiveness in accommodating target analytes partly rely on the surface area, porosity, and functional groups of the adsorbing material; the abundance of these properties positively influences the adsorption performance. Several metal oxides, activated carbon, biochar, and zeolite have been applied to remove metal ions from water [16–19]. Despite their good adsorption performances, these materials still suffer from poor adsorption towards anionic metal ions, as their functional groups mostly target positively charged trace elements. Layered double hydroxides (LDHs) are emerging as suitable materials for the adsorptive removal of various trace elements from water without discrimination because of their unique layered structure and fascinating ion-exchange capabilities [20–23]. LDH have positively charged brucite-like layers, exhibiting a general formula $[M^{2+}_{(1-x)}M^{3+}_{x}(OH)_2]^{x+}[(A^{n-})_{x/n}\bullet yH_2O]^{x-}$, with M^{2+} and M^{3+} as divalent and trivalent metal cations, respectively, and A^{n-} as an interlayer anion, as shown in Scheme 1 [24]. The anionic heavy metal(loid) is usually adsorbed via anionic exchange and occupies the interlayer region of LDH [25]. However, this mechanism sometimes suffers from a loss of effectiveness due to interlayer anions that strongly bind to the interlayer region and resist interchange with targeted anionic metal(loid)s.

One of the structural properties of LDH is the ability to be calcined at higher temperatures to eliminate the intercalated anions and water molecules, thus collapsing the lamellar structure and producing layered double oxides (LDO) with even larger adsorptive sites, as shown in Scheme 1. The large adsorptive sites may be attributed to the thermal treatment process, which increases the porosity and specific surface area [26, 27]. Additionally, LDO can reconstruct to its original LDH structure when hydrated in solution containing anionic species; this renders them suitable to remove anionic metal(loid) species such as Cr(VI) and As(V) from water, which forms part of the regenerated LDH structure in the interlayer region [28–30]. As a result, this employed LDO for the adsorptive removal of anionic and cationic metal(loid)s from water to address the drawbacks associated with the parent LDH.

This study aimed to prepare Fe-Zn-Al LDO as an adsorbent for removing As(III), Cd(II), and Pb(II) species from the surface and groundwater samples collected from the Eastern Cape Province. Fe-Zn-Al LDO adsorbent was synthesised via calcining the Fe-Zn-Al LDH at higher temperatures. The Fe-Zn-Al LDO was characterised to determine the functional group, elemental composition, morphology, particle sizes, textural properties, and surface charge by using. The central composite design (CCD) was used to optimise the effect of pH and mass of adsorbent (MA) on the removal of As(III), Cd(II), and Pb(II) species from

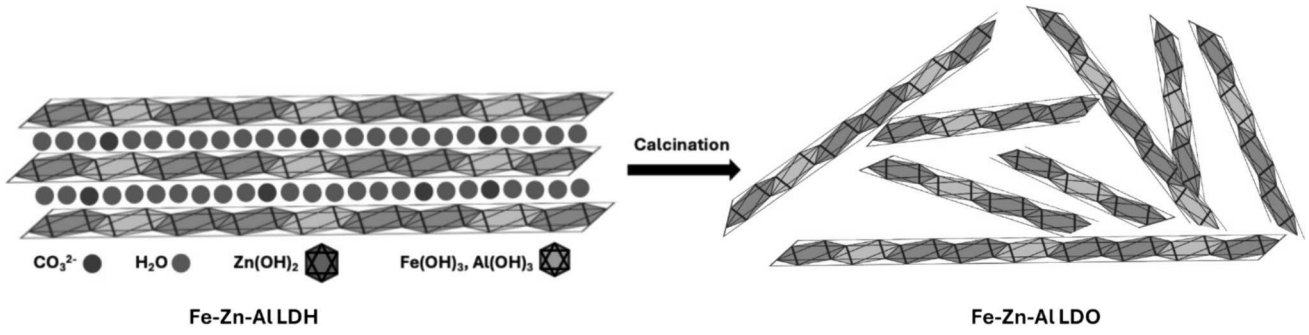

Scheme 1 Schematic diagram of the hydrotalcite

simulated water. The kinetics and isotherm studies were evaluated under optimum conditions. The performance of Fe-Zn-Al LDO adsorbent in removing As, Cd and Pb in groundwater and surface water spiked with a concentration of 1.0 mg/L was assessed. This contributed towards developing sustainable materials for effectively eliminating harmful pollutants from water sources in rural areas, thus promoting water resource protection.

2 Experimental

2.1 Chemicals and reagents

Aluminium nitrate nonahydrate ($Al(NO_3)_3{\cdot}9H_2O$, 98% purity), zinc nitrate hexahydrate ($Zn(NO_3)_2{\cdot}6H_2O$, 98% purity), iron nitrate nonahydrate ($Fe(NO_3)_3{\cdot}9H_2O$, 98%), sodium carbonate (Na_2CO_3, 99% purity), sodium hydroxide (NaOH, 99%) were bought from Sigma Aldrich. The standard solutions of 1000 mg/L lead (Pb), Arsenic (As) and cadmium (Cd) were purchased from Merck (Johannesburg, South Africa) and ultra-pure water, which was used as the solvent, ammonia (NH_3) solution, and 65% nitric acid (HNO_3).

2.2 Synthesis of Fe-Zn-Al LDH

Fe-Zn-Al LDH was synthesised utilising the co-precipitation synthetic technique. In detail, metal salts, 2.33 g $Fe(NO_3)_3.9H_2O$, 3.40 g $Zn(NO_3)_2{\cdot}6H_2O$, and 1.70 g $Al(NO_3)_3{\cdot}9H_2O$, were transferred in 80 mL ultrapure water for dissolution. Separately, 7.95 g Na_2CO_3 was dissolved in 25 mL ultrapure water to prepare a 3 mol alkaline solution. The alkaline solution was added to a stirring solution of mixed metals dropwise. The pH of the resulting solution was adjusted to 9 with 0.1 M NaOH, which was followed by aging the mixture while stirring under reflux at 80 °C for 18 h. Eventually, the produced brown precipitate of Fe-Zn-Al LDH was filtered and washed with excess ultrapure water to remove any unreacted materials. Subsequently, it was dried in a vacuum oven at 80 °C for 24 h. The synthesis steps are presented in Scheme 2.

2.3 Synthesis of Fe-Zn-Al LDO

The Fe-Zn-Al LDO was synthesised by calcining the pre-synthesised Fe-Zn-Al LDH (as described in Sect. 2.2). Briefly, the preprepared Fe-Zn-Al LDH was transferred into a ceramic crucible and placed in the muffle furnace. The furnace was allowed to heat to 400 °C, then maintained at that temperature for 3 h. After calcination, the Fe-Zn-Al LDO was allowed to cool to room temperature. The synthesis of LDO is represented by a schematic diagram in Scheme 2.

2.4 Instrumentation

The functional groups of Fe-Zn-Al LDO were studied using the Fourier transform infrared (FTIR) spectrometer (Waltham, MA, USA). The technique employed KBr, which was mixed with the sample at a 1:10 ratio to make a pellet. The prepared KBr pellet was placed into the instrument for analysis. The Philips X-ray generator model PW 3710/31 X-ray diffraction (XRD) was used to analyse the crystallinity of the materials operating with Cu-Kα X-ray (λ = 1.54060 Å), recording at a 2θ range of 2.0–90°, and operating at a scan speed of 66.045 s. The dimension and morphology of the material were confirmed with a transmission electron microscope (TEM), JEM 2100, JEOL Co. Japan, with an operating

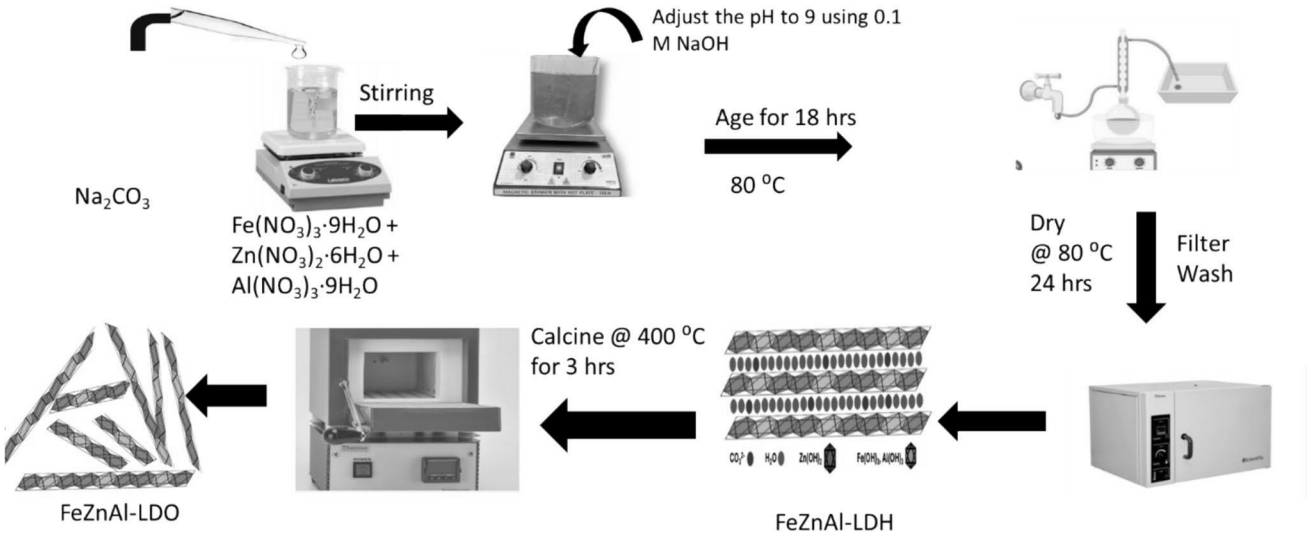

Scheme 2 Diagram showing a schematic representation of the synthesis of LDH and LDO

voltage of 200 kV. Scanning electron microscope, TESCAN VEGA 3 xmu, LMH of the Czech Republic, in tandem with Energy dispersive X-ray spectroscopy (SEM–EDX), was used to determine the elemental composition in Fe-Zn-Al LDO. The surface charge of the material was analysed utilising Nano-ZS Zetasizer (Malvern Instruments, Malvern, UK). The sample was prepared by suspending 30 mg of Fe-Zn-Al LDO in 500 mL ultrapure water, and then adjusting the pH to a range of 2.0–12 using 0.1 M HCl and NaOH solutions. The samples were sonicated for 1 h at room temperature before analysis. The BET surface area, pore diameter and the average pore size of the Fe-Zn-Al LDO were studied using N_2 and CO_2 adsorption–desorption analysis. The analysis was conducted using an Anton Paar BET surface area analyser (Nova 800) fitted with 21 CFR Part 11-compliant software. The pH was measured using a Bante 901 Benchtop pH meter. The material was calcined utilising a Thermo Scientific Thermolyne benchtop MX8-13TP muffle furnace. The ultrasonication to facilitate the adsorption and dispersion of Fe-Zn-Al LDO was performed using a SciTech ultrasonic bath system with a 50 Hz frequency and 150 W power (Labotec, Midrand, South Africa). Inductively coupled plasma-optical emission spectrometry (ICP-OES) (iCAP 6500 Duo, Thermo Scientific) coupled with a charge injection device (CID) detector to detect and quantify As, Cd, and Pb.

2.5 Batch adsorption study

The adsorption efficiency of Fe-Zn-Al LDO was assessed via a batch adsorption study. The 1000 mg/L standard As(III), Cd(II) and Pb(II) solutions were employed to prepare working solutions and calibration standards. The 1.0 mg/L concentration of a mixture of metal(loid)s was prepared by diluting a specific volume of a standard solution with ultrapure water. The calibration standards with a 0.5–55 mg/L range were also prepared similarly. The pH of the solution was adjusted with 0.1 M HCl and 1.0 mol/L ammonia solution to pH values in the range 1.369–8.630. The batch adsorption was conducted at room temperature by adding 20 mL of the sample solution into 50 mL centrifuge tubes containing the required amounts (11.6–108.4 mg) of Fe-Zn-Al LDO. The solution mixtures were sonicated for 30 min, followed by the separation of the supernatant with a 0.22 μm PVDF filter. The supernatant and the synthetic samples were analysed for equilibrium and initial concentration of Cd and Pb using ICP-OES.

2.5.1 Optimisation of batch adsorption

The optimisation of batch adsorption is important as it helps maximise the adsorptive removal of contaminants. The central composite design (CCD) was utilised to optimise the adsorptive removal of As(III), Cd(II) and Pb(II) by varying the solution pH in the range 1.37–8.63 and the mass of Fe-Zn-Al LDO (in the range 11.6–108.4 mg). The choice of the parameters was influenced by preliminary studies that showed that pH and mass of adsorbent played a critical role in the adsorption process. The adsorption process was conducted similarly to that described in Sect. 2.5. When the adsorption separation step was complete, the supernatant was quantified with ICP-OES and the results were used to calculate the removal efficiency (%RE) and adsorption capacity (q_e) of the adsorbent using Eqs. (1) and (2) below, respectively:

$$\%RE = \frac{(C_0 - C_e)}{C_0} \times 100\% \tag{1}$$

$$q_e \frac{(C_0 - C_e)\,V}{m} \tag{2}$$

where C_0, C_e, m, and V are initial and equilibrium concentrations of analytes, mass of adsorbent, and sample volume, respectively.

2.5.2 Adsorption isotherm

Here, the batch adsorption was conducted by varying initial concentrations of the mixture of As(III), Cd(II) and Pb(II) in the range 1.0–50 mg/L with a sample volume of 100 mL and an adsorbent mass of 20 mg. The pH of the metal(loid) solution was adjusted to 6.5 using 1 mol/L ammonium solution or 0.1 mol/L HCl. After adsorption, the experimental data were fitted into two isotherm models to understand the mode of interaction between the Fe-Zn-Al LDO and As(III), Cd(II) and Pb(II).

Langmuir isotherm model:

$$q_e = \frac{q_{max} K_L C_e}{1 + K_L C_e} q_e \tag{3}$$

In which q_e (mg/g), q_{max} (mg/g), C_e (mg/L), and K_L (L/mg) are the equilibrium adsorption capacity, maximum adsorption capacity, concentration of metal(loid)s at equilibrium, and isotherm constant that represents the affinity of adsorbent on the adsorbate, which can be used for calculation of the separation factor (R_L) using Eq. (4).

$$R_L = \frac{1}{1 + K_L C_i} R_L \tag{4}$$

Freundlich isotherm model:

$$q_e = K_F C_e^{1/n} q_e \tag{5}$$

where q_e (mg/g) is the amount of adsorbed metal(loid)s per given mass of Fe-Zn-Al LDO, K_F (mg/g) is the coefficient of the Freundlich constant, n is the adsorption intensity parameter, and C_e (mg/L) is the concentration of metals at equilibrium.

2.5.3 Adsorption kinetics

The effect of contact time on the adsorption of As(III), Cd(II) and Pb(II) by Fe-Zn-Al LDO adsorbent was investigated, varying the adsorption time. This experiment was conducted via batch adsorption as in Sect. 2.5, but the adsorbent mass, sample volume, sample concentration, and sample pH were 20 mg, 100 mL, 50 mg/L, and 6.7, respectively. The adsorption process was facilitated for 5.0–60 min, followed by filtering of the supernatant using a 0.22 µm PVDF filter before analysis with ICP-OES. The kinetic data were fitted into nonlinear kinetic models, including pseudo-first order, pseudo-second order, Elovich and intraparticle diffusion, to better understand the adsorption mechanism and the rate-determining step. The equations used are presented below:

Pseudo first order:

$$q_t = q_e(1 - expt^{k_1 t}) \tag{5}$$

Pseudo second order:

$$q_t = \frac{k_2 q_e^2}{1 + k_2 q_e t} \tag{6}$$

Elovich model:

$$q_t = \frac{1}{\beta}\ln(\alpha\beta t + 1) \tag{7}$$

Intra-particle diffusion:

$$q_t = k_i t^{1/2} + C \tag{8}$$

where q_t (mg/g) is the amount of sorbate adsorbed at time t, q_e is the adsorption capacity at the equilibrium. The k_1 (min^{-1}), k_i ($mg/g/min^{-1/2}$), and k_2 (g/mg·min) are the adsorption rate constants for pseudo-first order, Intra-particle diffusion, and pseudo-second order, respectively. Parameters β ((g/mg), α (mg/g·min), and C (mg/g) are the desorption constant, initial adsorption rate, and constant providing information about the boundary of the layer thickness, respectively.

2.5.4 Adsorption thermodynamics studies

The thermodynamic studies followed the optimised adsorption method by varying the temperature from 25–40 °C. All experiments were performed in triplicate, and the results were reported as the means of the three replicates.

2.6 Application to actual water samples and reusability studies

Fe-Zn-Al LDO was evaluated for the adsorptive treatment of water samples containing As, Cd, and Pb, which were collected from King Sabatha Dalidyebo Local Municipality, Eastern Cape, namely Eluxolweni tap (ELX-T) water, Eluxolweni dam (ELX-D), Emavundleni dam (EMD-D), Emavundleni stream (EMD-ST), and Gubevu stream (GBV-ST) in Eastern Cape province. Trace metal(loid) species such as As(III), Cd(II) and Pb(II) concentrations in actual water samples were present in trace levels. Therefore, 20 mL water samples were spiked with 1.0 mg/L of a mixture of As(III), Cd(II) and Pb(II), and transferred into 50 mL centrifuge tubes containing 20 mg of Fe-Zn-Al LDO to evaluate the applicability of the adsorbent in a real application. The sample mixtures were sonicated for 30 min, filtered using a 0.22 µm PVDF filter to separate the supernatant before analysis with ICP-OES.

Under optimised conditions, the reusability and regeneration experiments were carried out by performing several adsorption–desorption cycles. This was achieved by desorbing the As(III), Cd(II) and Pb(II) species adsorbed on the Fe-Zn-Al LDO surface using 0.1 mol/L nitric acid. The Fe-Zn-Al LDO was washed with deionised water 3 times and rinsed with ethanol three times. The adsorbent was dried in an oven for 2 h, and the spent adsorbent was reused in the successive adsorption–desorption cycles. The same procedure was repeated five times.

3 Results and discussion

3.1 Characterisation of the synthesised Fe-Zn-Al LDO material

3.1.1 Functional groups and crystallinity of Fe-Zn-Al LDO

Figure 1(a) shows the FTIR spectra of Fe-Zn-Al LDH and Fe-Zn-Al LDO. The spectrum of Fe-Zn-Al LDO shows intense peaks at 3410–3556 cm^{-1}, which are stretching vibration bands of O–H, attributed to the O–H of water molecules. The band at 1636 cm^{-1} was assigned to the H–O-H stretching vibration. The peaks at 1400 cm^{-1} and C-O are attributed to the vibrations of C=O and C-O of the CO_3^{2-} anion, which was intercalated in the interlayer of Fe-Zn-Al LDH, as also evident on the spectrum of Fe-Zn-Al LDH. This suggests that CO_3^{2-} was not entirely removed during the thermal treatment at 400 °C. This may be ascribed to the

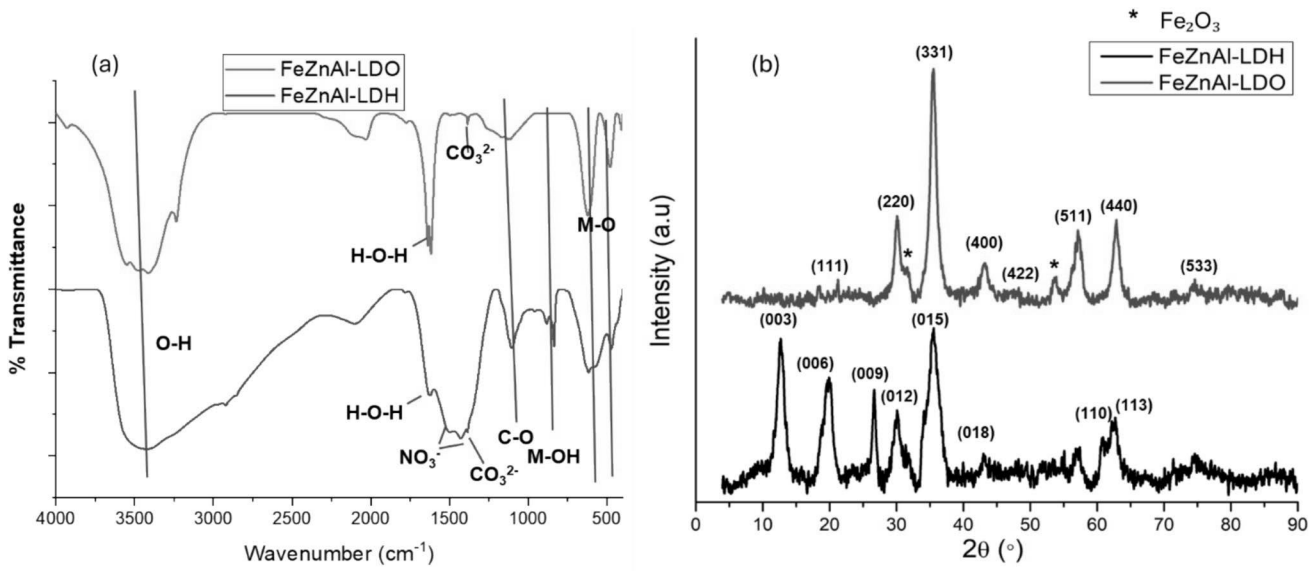

Fig. 1 (**a**) FTIR spectra and (**b**) the X-ray diffractograms for Fe-Zn-Al LDH and Fe-Zn-Al LDO

high stability of CO_3^{2-}, which forms a stronger affinity with positive layers because it is a divalent anion. This is supported by the study by Ref [31], which demonstrated that after calcining LDH to temperatures up to 500 °C, CO_3^{2-} was still present. At the same time, extremely high temperatures can permanently denature the material and prevent it from reconstructing to the original layered double hydroxide structure [32]. The intense stretching vibration peaks at 1432 cm^{-1} assigned to NO_3^- anion on the spectrum of Fe-Zn-Al LDH completely disappeared on the spectrum of Fe-Zn-Al LDO after thermal treatment. This phenomenon is owed to the fact that it is not tightly held in the interlayer region as it was with CO_3^{2-} [33]. The spectrum of Fe-Zn-Al LDH shows peaks at 465, 611 and 850 cm^{-1}, which are stretching vibrational bands of M–O, M–O-M and M-OH, where M = Fe, Zn and Al, which confirms the successful formation of Fe-Zn-Al LDO adsorbent.

The diffraction patterns of Fe-Zn-Al LDH and Fe-Zn-Al LDO are represented in Fig. 1(b). The diffractogram of Fe-Zn-Al LDH showed a typical diffractogram of hydrotalcite-like materials (JCPDS 14–191), with diffraction peaks at 2θ = 12.6, 19.7, 26.4, 30.3, 35.7, 43 and 63, which correspond to (003), (006), (009), (012), (015), (018), (110) and (113) diffraction planes, respectively. The diffraction planes (003), (006), and (009), which are present on the diffractogram of Fe-Zn-Al LDH and are characteristics of a double-layered structure of LDHs, disappeared after thermal treatment. This means the LDH precursor lost its lamellar character because of calcination and removal of water and carbonate species, which further confirms the successful formation of Fe-Zn-Al LDO [34]. As a result, new reflections characteristic of crystalline mixed oxides emerged. The most dominant peak among these was the (311) plane of spinel $ZnFe_2O_4$ at 36.4°. There are other additional reflections at ~ 30.6° (220), ~ 43.8° (400), and ~ 63.5° (440). These findings confirm the formation of a cubic spinel structure for the $ZnFe_2O_4$ nanoparticles according to the JCPDS card No. 82–1042 [35]. There is also an indication of peaks corresponding to Fe_2O_3 and ZnO in the calcined LDO, however, most of these peaks overlap with the ones for spinel $ZnFe_2O_4$. The observed structural reconstruction of LDH to LDO is consistent with the established thermal decomposition pathway of layered double hydroxides, in which dehydration and dehydroxylation are followed by recombination of metal cations into stable oxide lattices.

3.1.2 Elemental composition and morphology of Fe-Zn-Al LDO

Figure 2(a) shows the area where the EDS spectrum for Fe-Zn-Al LDO was obtained, and the spectrum confirmed Fe, Zn, Al, and O elements (Fig. 2(a)). These results are consistent with the functional groups of Fe-Zn-Al LDO that were characterised by FTIR (Fig. 1(a)). This confirms that both materials were of high purity since no other elements were detected. Figure 2(c) shows that Fe-Zn-Al LDO has spherically shaped particles with a size of 12 ± 2 nm (the yellow line across the diameter of the spherical particles demonstrates how the sizes were measured using Image J software). The TEM images also confirm that LDO exhibit spherical morphology.

3.1.3 Textural properties and point of zero charge

The CO_2 and N_2 adsorption–desorption analysis was used to determine the surface area, pore volume and pore diameter

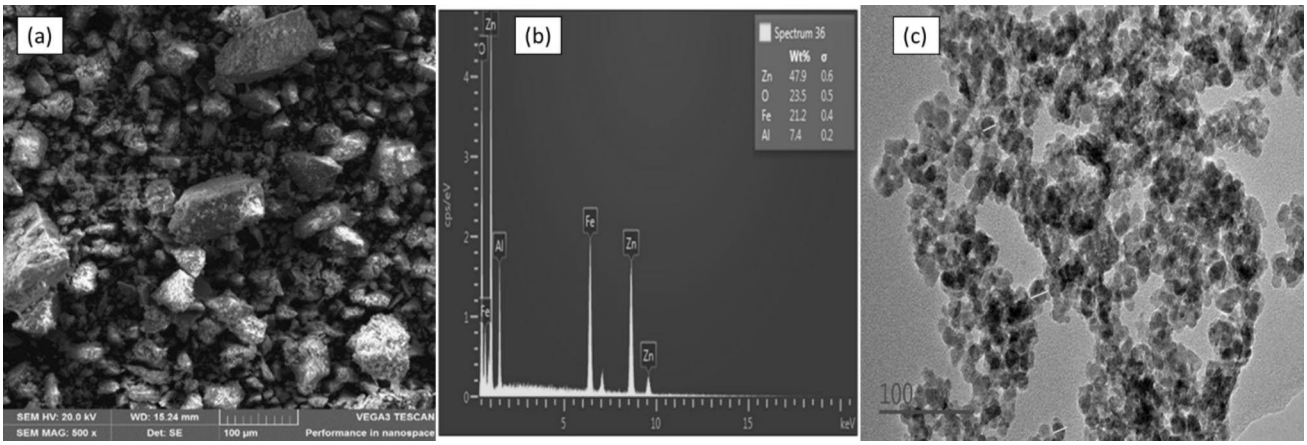

Fig. 2 (**a**) SEM image, (**b**) Energy dispersive X-ray spectrum and (**c**) TEM image of Fe-Zn-Al LDO

of Fe-Zn-Al LDO. Figure 3(a) revealed that Fe-Zn-Al LDO has a type IV isotherm, representing mesoporous structure materials [36]. The H1 hysteresis loop supports the presence of mesopores. The pore size distribution in Fig. 3(b) indicates the presence of micropores, with pore diameters of 0.349 nm, 0.57 nm and 0.789 nm. Meanwhile, the Barrett-Joyner-Halenda (BJH) pore size distribution in Fig. 3(c) shows peaks at 7.5 and 18.5 nm, which are attributed to mesopores. The results also showed that Fe-Zn-Al LDO consists of mesopore and micropore structures. Fe-Zn-Al LDO exhibits a large Brunauer–Emmett–Teller (BET) surface area and pore volume of 88 m^2/g and 0.35 cm^3/g, respectively.

Figure 3(d) represents the zeta potential for Fe-Zn-Al LDO, which was obtained at different pH values in the range of 2.0–12. The point of zero charges (pH_{PZC}) is pH where the surface charge density is neutral, and the zeta potential of the material is zero. The pHPZC of Fe-Zn-Al LDO is 9, and it can be observed that at pH below 9, the surface of Fe-Zn-Al LDO becomes positively charged and negatively charged when the pH is above 9. The adsorptive decontamination of As(III) is anticipated to be favoured at pH below 9 since it is anionic. In contrast, Cd(II) and Pb(II) adsorption is expected to dominate at pH above 9 because they are cationic. The anticipated mechanism includes interlayer intercalation, surface complexation and ion exchange [7, 37].

3.2 Optimisation of the adsorption process

This study used the CCD effect of sample pH and MA on the adsorptive removal of As(III), Cd(II) and Pb(II) by Fe-Zn-Al LDO adsorbent. The CCD matrix consists of 12 experiments, and the resulting analytical response values (% removal efficiency) are shown in Table 1. The data in Table 1 were analysed using analysis of variance (ANOVA) to investigate the main and interactive effects. The ANOVA results reproduced as Pareto charts are shown in Fig. 4(a-c).

The Pareto chart allows the visualisation of factors by arranging them along the x-axis in the order of importance, from most to least influential parameter. The longer the length of each bar, the greater the influence of each assessed variable on the interaction of the Fe-Zn-Al LDO and As(III), Cd(II) and Pb(II), and the vertical line shows a significant influence at a 95% confidence level [38]. Furthermore, the parameters are significant when the bar passes the line ($p = 0.05$) [39]. It can be observed in Fig. 4(a) that pH and MA were not significant, suggesting that increasing or decreasing these parameters did not negatively influence the adsorption of As onto Fe-Zn-Al LDO. However, the positive effect of MA and pH suggests that better removal efficiency was achieved when these parameters were slightly increased from the lowest to the highest (Fig. 4(a)). On the other hand, the adsorption of Cd and Pb onto Fe-Zn-Al LDO adsorbent was positively influenced by pH at a 95% confidence level. Even though the bar length representing MA did not cross the confidence line ($p = 0.05$), as shown in Fig. 4(b, c), the positive effects suggest that increasing MA increases the adsorption efficiency of the adsorbent.

3.2.1 Three-dimensional response surface plot

The 3D response surface plots showing the interactive effect of pH and MA on the adsorption of As(III), Cd(II) and Pb(II) onto Fe-Zn-Al LDO adsorbent are presented in Fig. 5(a-c). Figure 5(a) shows that the %RE for As(III) increases with increasing MA and pH. This phenomenon is owed to the positively charged surface of Fe-Zn-Al LDO at pH values ranging from 1 to 8.5, thus facilitating enhanced removal of anionic As(III) through electrostatic attraction [40]. However, as the sample pH increases, the charge of the material becomes less positive, moving

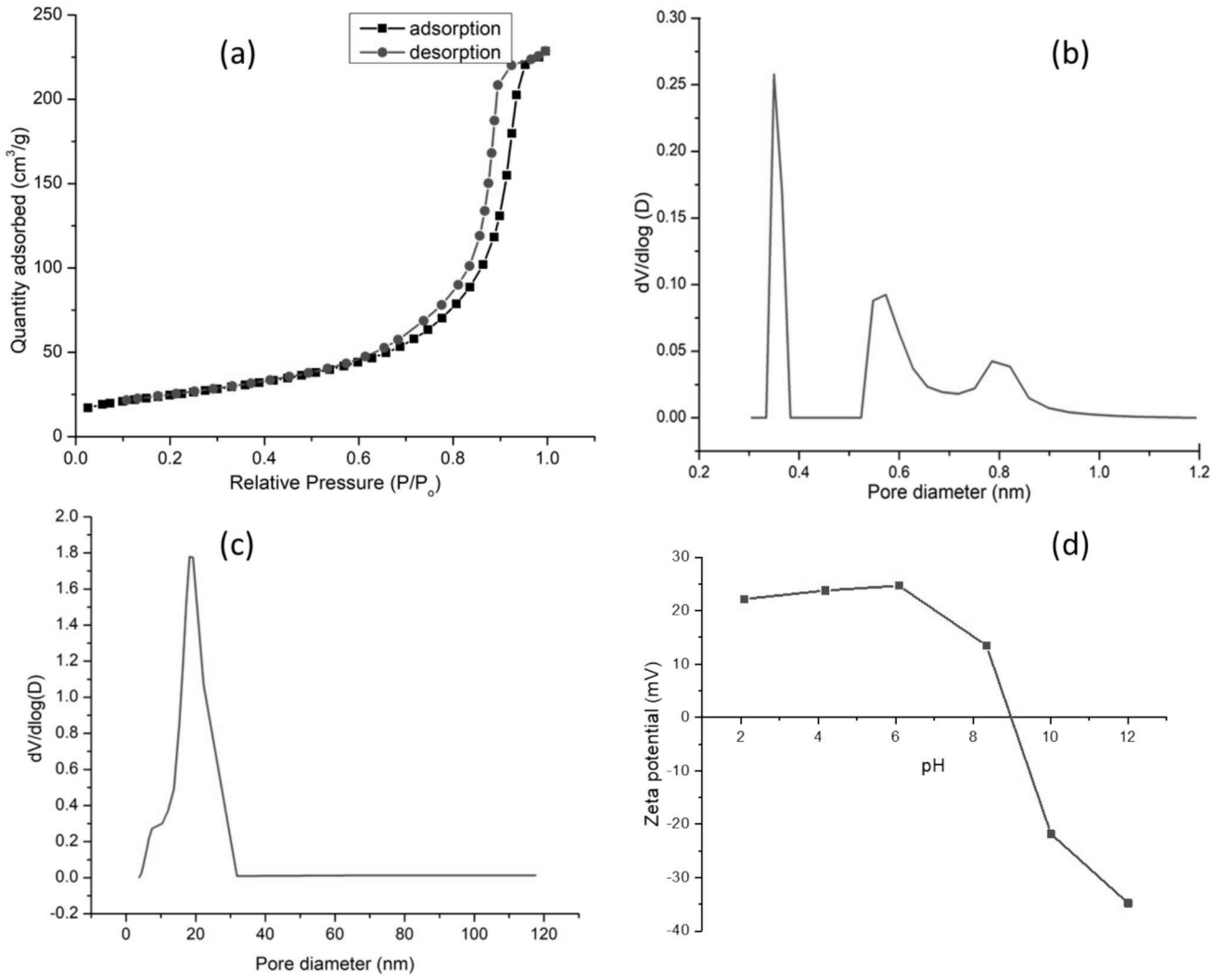

Fig. 3 (**a**) N_2 adsorption–desorption isotherm, (**b**) pore size distribution determined using CO_2 adsorption, (**c**) BJH pore size distribution (desorption branch) determined using N_2 adsorption, and (**d**) zeta potential for Fe-Zn-Al LDO

Table 1 The central composite design with % removal efficiency

Standard Run			% Removal efficiency		
	pH	MA(mg)	As(III)	Cd(II)	Pb(II)
1	2	20	94.8	86.6	87.2
2	2	100	98.0	95.3	97.1
3	8	20	91.5	99.6	98.9
4	8	100	97.7	99.7	99.6
5	1.37	60	85.2	75.9	71.6
6	8.63	60	94.4	99.7	98.7
7	5	11.6	91.7	79.3	98.2
8	5	108.4	95.2	99.9	98.3
9 (C)	5	60	96.8	99.9	97.1
10 (C)	5	60	95.7	99.7	98.9
11 (C)	5	60	97.3	99.6	97.6
12 (C)	5	60	96.0	99.7	98.8

towards pH_{PZC}, which weakens the electrostatic attraction mechanism. This happens as the LDO reconstruct to form LDH via the "memory effect", where anionic As(III) intercalates on the interlayer region, balancing the charges of the positive layers [26, 41]. Figure 5(b, c) showed that as MA and the pH of the solution increased, the interactions between Cd(II) and Pb(II) with the adsorbent favoured an increase in the analytical response (%RE). The increase in the solution pH positively influenced the uptake of Cd(II) and Pb(II) with Fe-Zn-Al LDO. This is because in acidic conditions, the metal ions and hydronium ions compete for the available sites, and there is a possibility that Fe-Zn-Al LDO is dissolved, thus leading to low adsorption efficiency [42].

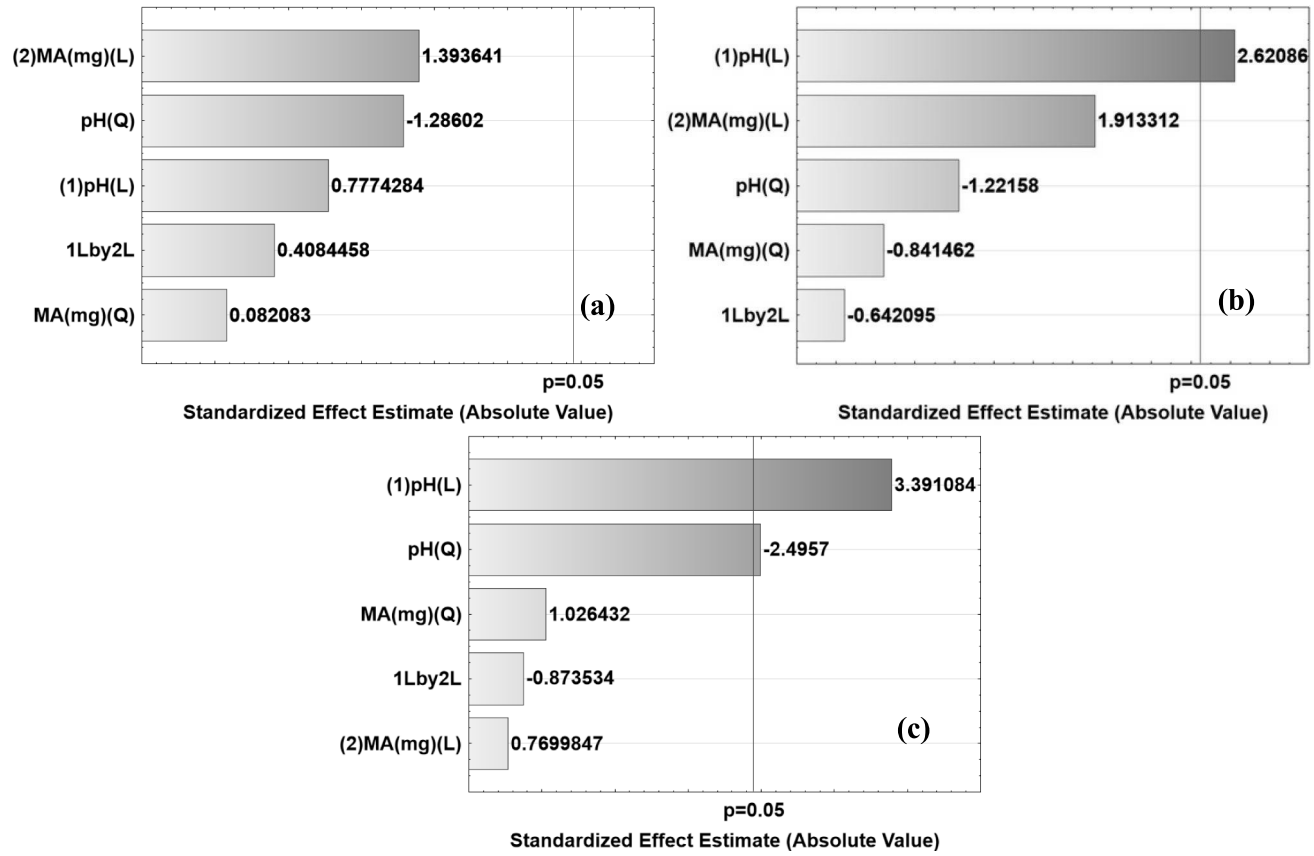

Fig. 4 Pareto charts showing the influence of pH and MA on the adsorption of (**a**) As, (**b**) Cd and (**c**) Pb by Fe-Zn-Al LDO

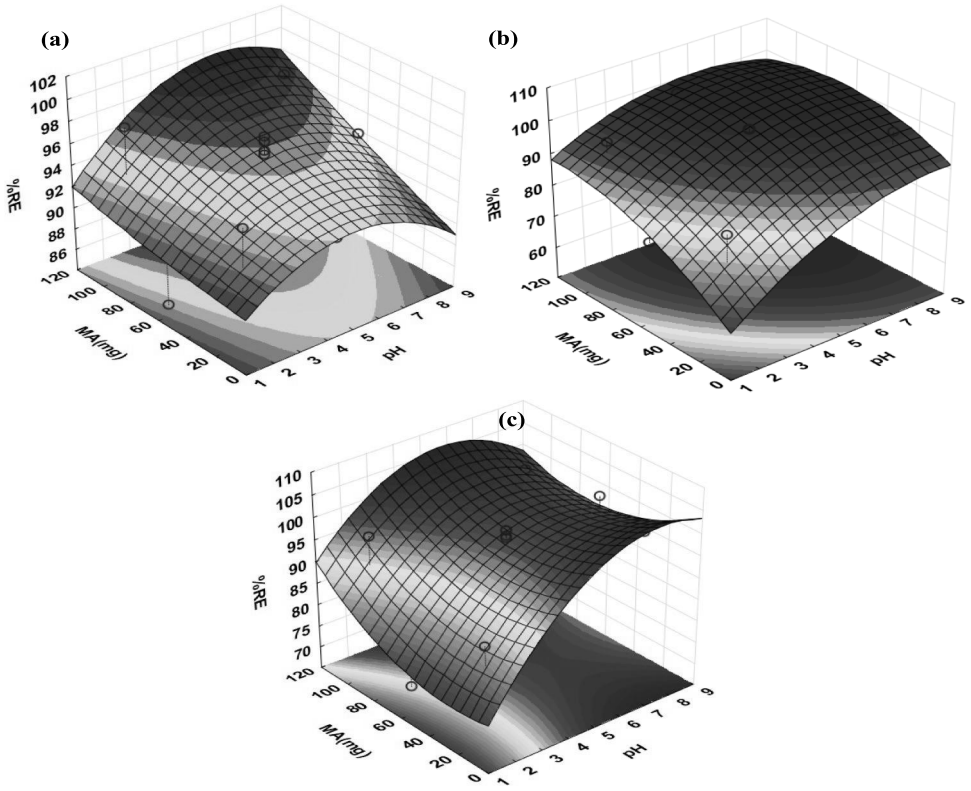

Fig. 5 3D response surface plot(s) for removing (**a**) Cd(II), (**b**) As(III) and (**c**) Pb(II) with Fe-Zn-Al LDO

According to Fig. 3(d), the surface of the adsorbent is positively charged at pH values < 9 (pH_{PZC} = 9). These results revealed that the electrostatic interaction between the target cations (Cd(II) and Pb(II)) and the positively charged adsorbent was not controlling the adsorption process. Therefore, the removal of Cd(II) and Pb(II) was governed by the coordination between the cations and the electron–ion pair of the oxygen atom on the Fe-Zn-Al LDO surface. The FTIR results revealed that the Fe-Zn-Al LDO adsorbent was composed of functional groups such as CO_3^{2-}, M–O, M–O-M and M-OH, which could also enhance the adsorption of the target on the surface of the adsorbent. Therefore, it was concluded that the adsorption of Cd(II) and Pb(II) was facilitated by complexation with functional groups (such as CO_3^{2-}, M–O, M–O-M and M-OH) on the Fe-Zn-Al LDO surface. In addition, the precipitation effect resulting from forming metal hydroxides or carbonates, due to Cd(II) and Pb(II) with the functional groups, enhanced the removal of Cd(II) and Pb(II).

3.2.2 Desirability function

The desirability function was applied to optimise independent variables further simultaneously, in which the anticipated responses are converted into a dimensionless desirability value, as shown in Fig. 6. The desirability values are D = 0, the minimum desirability value is 0.5, and the central point and D = 1, which is the maximum desirability value. These values were used to obtain the optimum solution pH and MA. As shown in Fig. 6, the optimum conditions are shown in the vertical red line at the maximum desirability value. According to these results, the optimum pH and MA conditions for As(III), Cd(II) and Pb(II) adsorption onto the Fe-Zn-Al LDO adsorbent were 6.8 and 108.4 mg, respectively. Figure 6(c) shows that 20 mg Fe-Zn-Al LDO could quantitatively adsorb the analytes. Therefore, a smaller mass (20 mg) of Fe-Zn-Al LDO was chosen based on cost-effectiveness and environmental friendliness. For an application in real samples, the pH of ground and surface waters often ranges from 6.0–8.5. Therefore, the adsorption

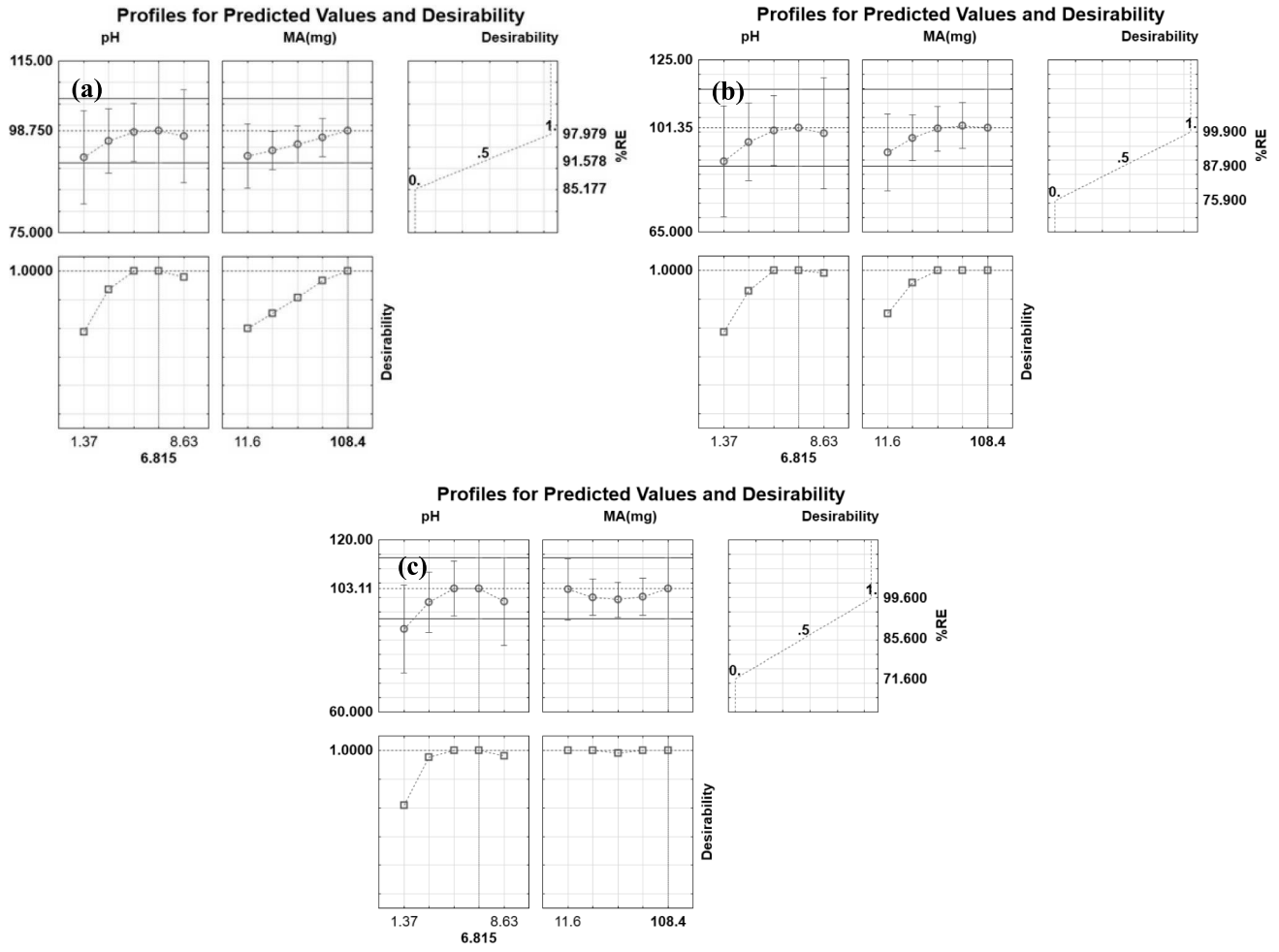

Fig. 6 The desirability plots for optimisation of AM and pH for adsorption of (**a**) Cd(II), (**b**) As(III) and (**c**) Pb(II) on Fe-Zn-Al LDO adsorbent

process was conducted in the subsequent experiments with an initial sample pH between 6.5 and 7.0. Also, it was observed that at pH values above 7, Cd(II) and Pb(II) start to precipitate in solution.

The predicted optimum conditions were verified by conducting six replicates of adsorption experiments. The experimental %R values for As(III), Cd(II) and Pb(II) were 99.1±3.1%, 98.9±4.3% and 99.6±4.1%, respectively. On the other hand, Fig. 6 shows that the predicted %R ranged from 98.8–103%. The experimental results were within the predicted %RE range, suggesting that the RSM model was valid.

3.3 Adsorption isotherm

The effect of metal(loid) initial concentrations on the adsorption of As(III), Cd(II) and Pb(II) with Fe-Zn-Al LDO was studied, and the results are shown in Fig. 7. As seen, the adsorption capacities of Fe-Zn-Al LDO for adsorption of As(III), Cd(II) and Pb(II) increased with increasing initial concentration. They then steadily attained a plateau at a higher initial concentration. The maximum experimental adsorption capacities were 225 mg/g, 196 mg/g and 247 mg/g for As(III), Cd(II) and Pb(II), respectively. The equilibrium data in Fig. 7 were employed to study the adsorption behaviour of As(III), Cd(II) and Pb(II) by fitting the data to Langmuir and Freundlich isotherm models. The respective parameters are presented in Table 2.

The Langmuir model is based on adsorption homogeneity, which is the availability of the monolayer active sites for uniform adsorption energy without cations interacting on the adsorbent surface. The Freundlich model is based on multilayer adsorption, with adsorbate interactions happening on the heterogeneous adsorbent surface. The values of n or 1/n are used to represent adsorption parameters like surface adsorption intensity; the process of adsorption is

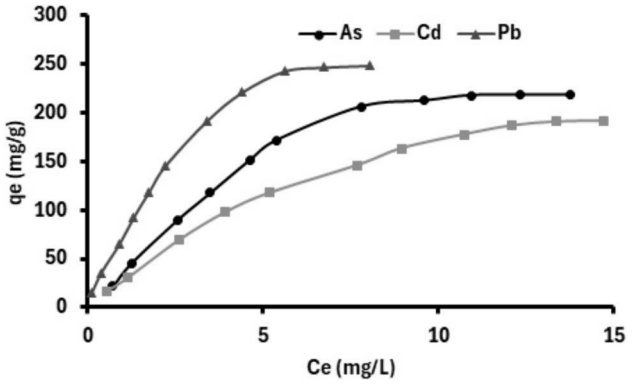

Fig. 7 Equilibrium data for As(III), Cd(II) and Pb(II) adsorption using Fe-Zn-Al LDO adsorbent. Conditions: MA = 20 mg; sample pH = 6.7; sample volume = 100 mL; contact time: 30 min

Table 2 The summary of the Freundlich and Langmuir models applied for the adsorption process of As(III), Cd(II) and Pb(II) with Fe-Zn-Al LDO

Isotherms		As(III)	Cd(II)	Pb(II)
$q_{experimental}$ (mg/g)		225	196	247
Freundlich	K_F(mg/g)	38.7	29.9	73.7
	1/n	0.76	0.75	0.67
	R^2	0.9400	0.9818	0.9862
Langmuir model	q_{max} (mg/g)	233	204	256
	K_L (L/mg)	0.21	0.16	0.42
	R^2	0.8957	0.9635	0.9672

favoured when 1/n > 0, then unfavoured when 1/n > 1 and irreversible for 1/n = 1 [43, 44]. Table 2 summarises the calculated parameters for the isotherm models for As(III), Cd(II) and Pb(II) adsorption onto Fe-Zn-Al LDO adsorbent. The results revealed that the adsorption process favoured the Freundlich isotherm model with a correlation coefficient of 0.9400, 0.9818 and 0.9862 for As(III), Cd(II) and Pb(II), respectively. These results suggested that the multilayer adsorption of the analytes takes place on the heterogeneous adsorbent surface-active sites. This might be attributed to interlayer electrostatic interactions and complexation with functional groups during the chemisorption on the surface on the surface of the adsorbent. Furthermore, the values of 1/n were 0 < 1/n < 1 for all analytes, indicating that the adsorption of As(III), Cd(II) and Pb(II) is highly favoured. The results showed that the affinity of Fe-Zn-Al LDO towards the analytes followed the trend: Pb(II) > As(III) > Cd(II).

The performance of the adsorbent for the removal of As(III), Cd(II) and Pb(II) was compared to some other LDO-based adsorbents, as seen in Table 3. The results showed that Fe-Zn-Al LDO had higher adsorption capacities or were comparable to other adsorbents. However, some adsorbents had very high adsorption capacities compared to Fe-Zn-Al LDO. This might be due to the functionalisation of the respective LDO, which leads to multiple steps or the use of high initial concentrations.

3.4 Adsorption kinetics

The adsorptive removal of As(III), Cd(II) and Pb(II) with Fe-Zn-Al LDO was studied by varying times in the 5.0–60 min range while keeping optimum experimental parameters constant. The adsorption kinetics of Fe-Zn-Al LDO were unveiled by investigating the effect of the contact time on the adsorption of As(III), Cd(II) and Pb(II) onto the Fe-Zn-Al LDO surface. As seen in Fig. 8, the adsorption of As(III), Cd(II) and Pb(II) at the initial concentration of 50 mg/L was taken up rapidly within 30 min. Afterwards, as contact time increased from 30 to 60 min, the adsorption rate slowed until the equilibrium was reached at 60 min. The kinetic data were fitted into kinetics models, pseudo-first order,

Table 3 Comparison of the maximum heavy metal ion removal capacities with other LDH-based adsorbents

Adsorbent	Experimental conditions				Adsorption capacity (mg/g)			Refs
	pH	Dosage (g/L)	Contact time (min)	Initial conc. (mg/L)	Cd	Pb	As	
LDO-PC	7	1	180	100	99.5	99.8		[45]
(Mg/Fe)LDO-ASB	5	0.5	1440	40–500	270	408		[46]
Mag-LDO/C	6	1	90	200–400	386	360		[7]
S-FLDO	4	1	720	10–1000	-	870	-	[47]
MgAl-LDO@S	2–6	1	720	100	208	632	-	[48]
SA-GCN-LDO	6	0.5	60	25	165	-	-	[37]
$MnO2/MgFe\text{-}LDO_{400}$	5	1	120	100	-	1063	-	[49]
Co-Al LDO/AC	6	2	420	50–600		25.1		[50]
AF-LDO	6	1	1440	1–200	10.4	9.56	12.0	[24]
MgAl-LDO	-	0.25	1440	500	1422	1337	-	[51]
MnO_2@LDO	5	05	1440	5–100	-	-	112	[52]
Mg-Fe-Al LDO	5.7	5	1440	10–100	-	-	305	[39]
MG/S-LDO	5	1	30	20–2500	-	656	-	[53]
Mg–Al LDO	8.6	5	1440	100	-	-	283	[54]
MnO_2/MgFe-LDO	2–12	1	5–3960	50	-	-	51,0	[55]
Fe-Zn-Al LDO	6.7	0.2	30	1- 50	233	204	256	This study

Magnetic –LDO/Carbon(Mag-LDO/C), sulfate-loaded flower-like LDO (S-FLDO), sodium alginate-graphitic carbon nitride -LDO(SA-GCN-LDO), Alfalfa biochar-LDO(AF-LDO), magnetic sulfur (S)-doped graphene-like carbon-LDO (MG/S-LDO), LDO- pectin (LDO-PC)

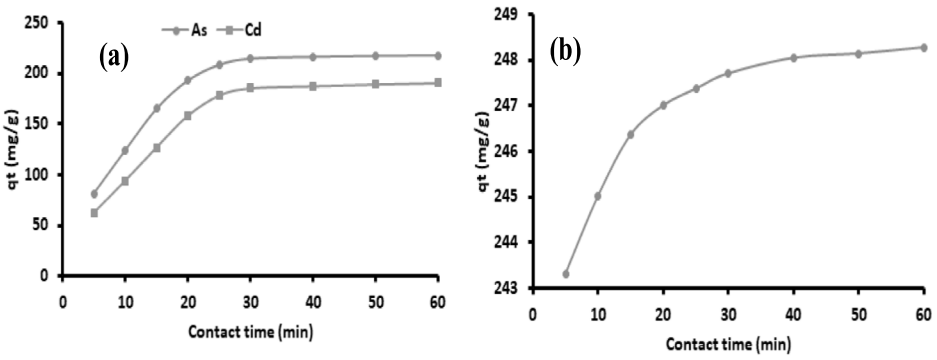

Fig. 8 Adsorption kinetics (**a**) of As(III) and Cd(II) and (**b**) Pb(II) onto Fe-Zn-Al LDO. Equilibrium data for As(III), Cd(II) and Pb(II) adsorption using Fe-Zn-Al LDO adsorbent. Conditions: MA = 20 mg; sample pH = 6.7; sample volume = 100 mL; contact time: 30 min

pseudo-second order, Elovich model and intra-particle diffusion, to understand the mechanism and the rate-determining step of the adsorption process.

The summarised kinetic model parameters are represented in Table 4. As shown in Table 4, the correlation of determination (R^2) for As(III), Cd(II) and Pb(II) adsorption onto the Fe-Zn-Al LDO adsorbent was more consistent with the pseudo-second-order model than the pseudo-first-order model. Furthermore, the adsorption capacities of the Fe-Zn-Al LDO adsorbent estimated from the pseudo-second-order model for all analytes agreed with the experimental q_e values. Table 4 shows that the pseudo-first-order model also described the adsorption of As(III) and Cd(II) onto the Fe-Zn-Al LDO surface since higher R^2 values were obtained. These results suggest that electrostatic interaction (in the case of As(III)) and ligand exchange (especially Cd(II)) coexist during adsorption. However, it is also clear that the adsorption of

Table 4 The summary of nonlinear kinetics model parameters for the adsorption removal of As(III), Cd(II) and Pb(II) with Fe-Zn-Al LDO

Models	Parameters	As(III)	Cd(II)	Pb(II)
Pseudo first order	q_e	181	192	97.9
	k_1	0.11	0.093	0.036
	R^2	0.9479	0.9641	0.9063
Pseudo second order	q_e	222	196	250
	k_2	0.0016	0.0024	0.027
	R^2	0.9879	0.9795	0.9998
Elovich model	α	59.2	87.7	2.93×10^4
	β	0.017	0.018	0.49
	R^2	0.9028	0.9223	0.9498
Intra-particle diffusion	$K_{i(1)}$	47.4	42.9	1.50
	$K_{i(2)}$	1.46	2.26	0.243
	C_1	23.6	37.2	240
	C_2	207	173	246
	$R^2_{(1)}$	0.9930	0.9943	0.9772
	$R^2_{(2)}$	0.9524	0.9971	0.9396

Pb(II) was strongly driven by chemisorption, and the adsorbent proved to have a high affinity toward Pb(II).

The Elovich model was used to understand the adsorption kinetics behaviour of As(III), Cd(II) and Pb(II) onto the surface of Fe-Zn-Al LDO. The adsorption of Pb(II) corresponded with the Elovich model ($R^2 = 0.9498$) compared to other analytes, as seen in Table 4. These findings demonstrate that film, heterogeneous and ion diffusions also governed the adsorption of Pb(II) in the pores of Fe-Zn-Al LDO. The intraparticle diffusion was used to state the rate-determining step for all analytes. The data showed that As(III), Cd(II) and Pb(II) adsorption occurred in multiple stages. The intraparticle diffusion graphs of all analytes did not begin at the origin, suggesting that boundary layer diffusion also affected the As(III), Cd(II) and Pb(II) adsorption. Therefore, As(III), Cd(II) and Pb(II) adsorption occurred in the first boundary layer, and subsequently, the intraparticle diffusion on Fe-Zn-Al LDO. The C values indicate boundary layer thickness (a significant value of C shows that the boundary layer has more effect) [56]. Table 4 shows that C values increased from 23.6–207 mg/g, 37.2–173 mg/g and 240–246 mg/g for As(III), Cd(II) and Pb(II), respectively. These values confirm that the boundary layer step determines the adsorption removal of As(III) and Cd(II), while the intraparticle diffusion stage controls Pb(II).

3.5 Adsorption thermodynamics studies

The effect of temperature on the adsorption of As(III), Cd(II) and Pb(II) onto Fe-Zn-Al LDO adsorbent was performed to confirm the sorption mechanism. The adsorption thermodynamic parameters such as standard Gibbs free energy change (ΔG°), enthalpy change (ΔH°) and entropy change (ΔS°) were estimated according to previous studies [57, 58]. Table 5 shows that the ΔG° values were negative, indicating the spontaneous adsorption of As(III), Cd(II) and Pb(II) onto Fe-Zn-Al LDO adsorbent. In addition, the positive ΔH° and ΔS° values for all analytes suggest that the adsorption process was endothermic and resulted in an increase in randomness (Table 5). These findings were attributed to structural changes of Fe-Zn-Al LDO adsorbent [58]. As shown in Table 5, the ΔH° values were greater than 20.9 kJ/mol, implying that the adsorption of As(III), Cd(II) and Pb(II) onto the adsorbent involved chemical interactions between the metal(loid) species and the Fe-Zn-Al LDO material [58].

Table 5 Thermodynamic parameters for adsorption of As(III), Cd(II) and Pb(II) onto Fe-Zn-Al LDO adsorbent

Temperature (K)	Analytes	ln*b*	ΔG° (kJ/mol)	ΔH (kJ/mol)	ΔS° (J/mol K)
298	As	0.21	−23.9	35.2	199
	Cd	0.16	−24.3	42.4	223
	Pb	0.42	−28.2	29.6	167
303	As	0.27	−25.1		
	Cd	0.19	−25.1		
	Pb	0.47	−28.9		
308	As	0.35	−26.1		
	Cd	0.28	−26.5		
	Pb	0.55	−29.8		
313	As	0.41	−26.9		
	Cd	0.35	−27.5		
	Pb	0.63	−30.7		

3.6 The evaluation of Fe-Zn-Al LDO adsorbent for the removal of As(III), Cd(II) and Pb(II) in real water

The adsorption performance and effectiveness of Fe-Zn-Al LDO adsorbent were examined in a real water medium to investigate its practicability and adsorptive removal behaviour under real surface water and groundwater conditions. High concentrations of major cations and anions and high turbidity characterised all water samples. As(III), Cd(II) and Pb(II) concentrations in ground and surface water samples ranged from 1.2–13.4 µg/L, 0.5–3.8 µg/L and 9.3–28.5 µg/L, respectively. The concentrations of As(III), Cd(II) and Pb(II) were below or above maximum permissible concentrations of 10 µg/L, 3 µg/L and 10 µg/L, respectively. When the adsorbent was applied in unspiked water samples, the concentrations of As(III), Cd(II) and Pb(II) after adsorption were below the detection limits of ICP-OES. Therefore, the water samples were spiked at concentrations higher than expected (1000 µg/L). Table 6 shows the removal efficiencies of As(III), Cd(II) and Pb(II) from surface water (streams and dams) and groundwater (boreholes). As shown, the removal efficiencies were below ≥ 90%, and the relatively low removal efficiencies might be due to the presence of major anions, which competed with the target analytes for the adsorption side. Despite these findings, the results in Table 6 suggested that the adsorbent can reduce As(III), Cd(II) and Pb(II) concentrations in contaminated water to levels within the maximum permissible concentration for

Table 6 The evaluation of As(III), Cd(II) and Pb(II) adsorption from real water samples from five different sides in Eastern Cape Province

Sites	%Removal efficiency		
	As(III)	Cd(II)	Pb(II)
ELX-T	85.3 ± 3.5	88.0 ± 3.6	89.8 ± 3.7
ELX-D	77.4 ± 3.2	75.3 ± 3.7	78.4 ± 4.1
EMD-D	73.0 ± 4.1	76.1 ± 4.1	80.1 ± 3.9
EMD-ST	75.6 ± 3.5	81.0 ± 4.2	87.6 ± 3.7
GBV-ST	87.4 ± 4.1	83.6 ± 3.7	88.2 ± 3.7

Eluxolweni tap (ELX-T) water, Eluxolweni dam (ELX-D), Emavundleni dam (EMD-D), Emavundleni stream (EMD-ST), and Gubevu stream (GBV-ST)

drinking water sources. Therefore, the synthesised Fe-Zn-Al LDO materials demonstrate sustainable feasibility in removing As(III), Cd(II) and Pb(II) from environmental water.

3.7 Adsorption mechanism

The possible adsorption mechanism between Fe-Zn-Al LDO and target metals (loid)s involves the electrostatic interaction of trace metal cations with the CO_3^{2-} that was not completely removed during calcination. The mechanism is supported by the increase in intensity of the peaks around 1400 cm^{-1}, attributed to the stretching vibration of the functional groups of CO32- in Fig. 9(a), compared to the almost insignificant peak in LDO before adsorption (Fig. 1(a)). The increase in intensity suggests that Cd(II) and Pb(II) coordinate to the LDO through the CO_3^{2-} functional group. Another major adsorption mechanism is the "memory effect" because of the reconstruction of LDO into LDH during adsorption. During reconstruction, LDO incorporates As(III) and CO_3^{2-} in the interlayer region, and the heavy metal cations bind through electrostatic interaction with the OH groups and CO_3^{2-}. The reconstruction of LDO into LDH is confirmed by the increase in intensity of the peaks attributed to OH, CO_3^{2-}, and C-O in Fig. 9(a) compared to Fig. 1(a), which is part of the double-layered hydroxide structure. Additionally, the formation of the peak attributed to M-OH, which is absent in the pure LDO (Fig. 9(a)), confirms the formation of Fe-Zn-Al LDH. The transformation of LDO into LDH was also confirmed by the formation of (003) and (006) diffraction planes (Fig. 9(b)), which are ascribed to the LDH structure, and were absent in the X-ray diffractogram of Fe-Zn-Al LDO (Fig. 1(b)) [59, 60].

3.8 Regeneration and reusability

The regeneration and reusability of Fe-Zn-Al LDO were investigated to assess its significant characteristics as a cost-effective and sustainable adsorbent for practical and real-world applications. The Fe-Zn-Al LDO recyclability was carried out by performing several adsorption–desorption experiments. The results demonstrated that the Fe-Zn-Al LDO absorbent had excellent adsorption performance within the first adsorption–desorption cycles (Fig. 10). The adsorption capacities for As(III), Cd(II) and Pb(II) decreased from 234–155 mg/g, 204–121 mg/g and 257–164 mg/g. The decrease in adsorption capacity through repeated adsorption–desorption cycles could be attributed to the disappearance of the memory effect with increasing adsorption–desorption cycles [61]. Although the adsorption efficiency of the Fe-Zn-Al LDO absorbent decreased with increasing adsorption–desorption cycles, its simple preparation, environmental friendliness, and cost-effectiveness make it an effective adsorbent.

4 Conclusion

This study successfully synthesised a low-cost and highly effective Fe-Zn-Al LDO material from Fe-Zn-Al LDH as a precursor via the calcination technique. The successful synthesis of the adsorbent was confirmed by FTIR, XRD, SEM–EDS and TEM, among others. Under optimum

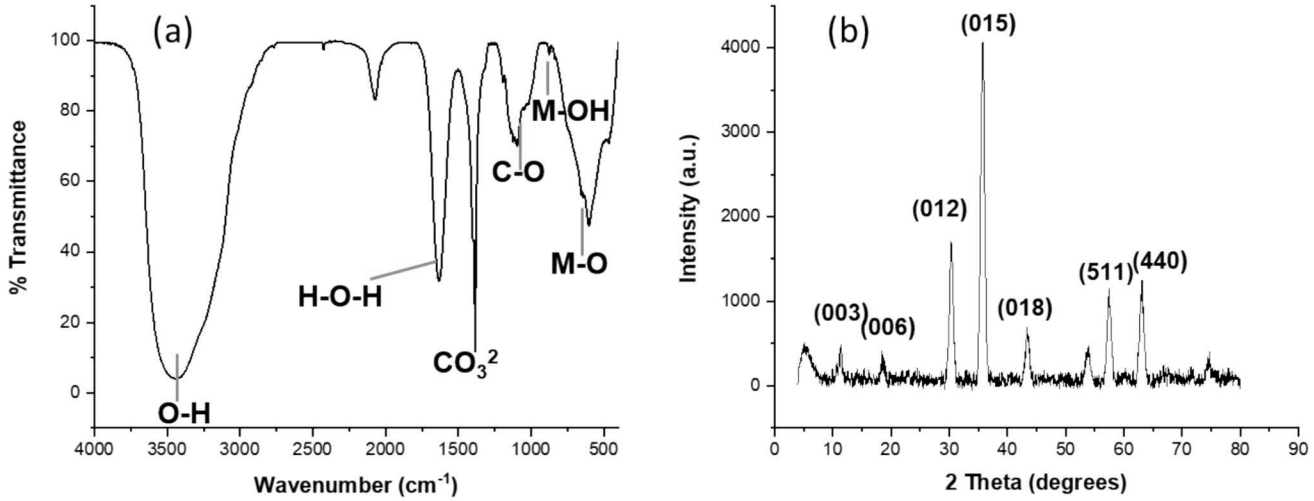

Fig. 9 FTIR spectrum and X-ray diffractogram of Fe-Zn-Al LDO post adsorption of As(III), Cd(II) and Pb(II)

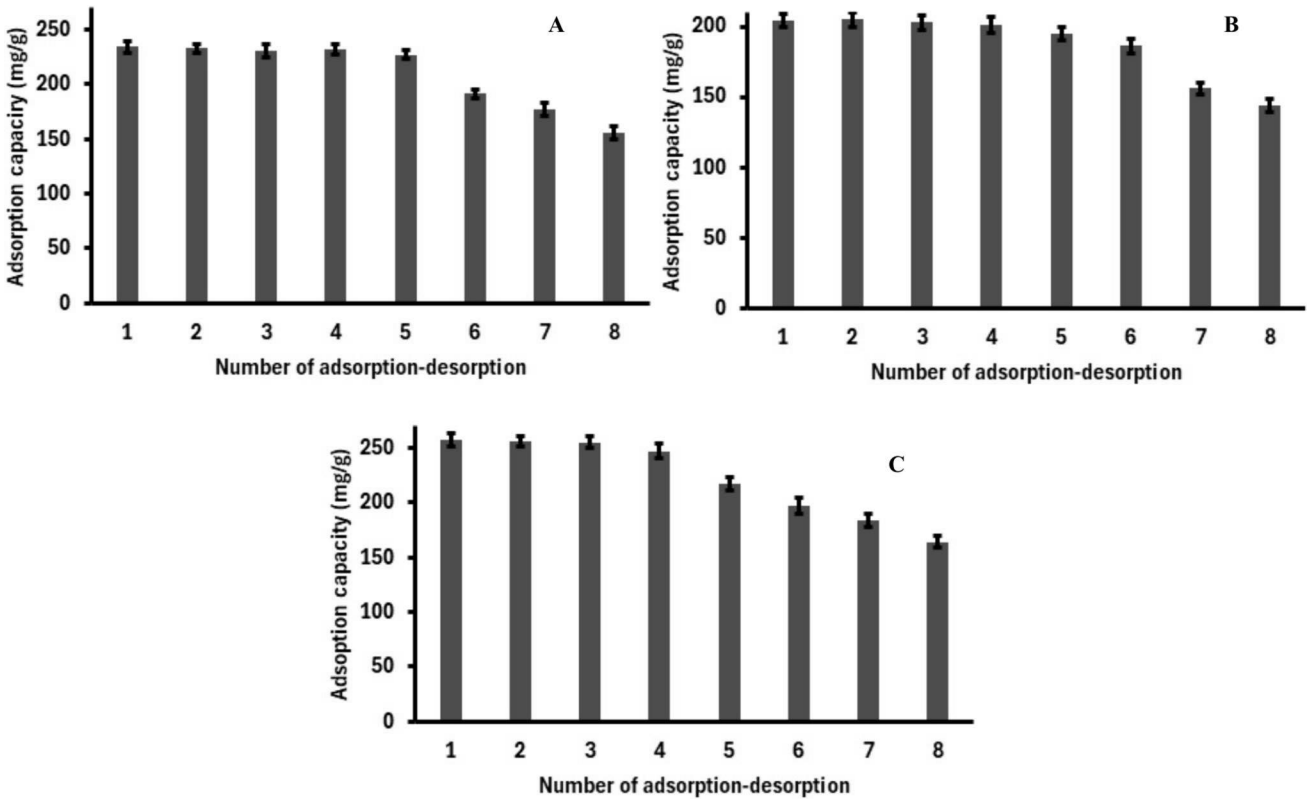

Fig. 10 The regeneration and reusability of the Fe-Zn-Al LDO adsorbent for the adsorption of (**a**) As(III), (**b**) Cd(II) and (**c**) Pb(II). Experimental conditions: adsorbent dose = 20 mg, pH = 7.0, 50 mg/L metal concentration, contact time = 30 min; all experiments were conducted at room temperature

conditions, the kinetic and equilibrium isotherm studies revealed that the adsorption of As(III), Cd(II) and Pb(II) was chemisorption on a heterogeneous surface of Fe-Zn-Al LDO material. In addition, the adsorption data showed that the affinity of Fe-Zn-Al LDO adsorbent towards the target analytes was Pb(II) > As(III) > Cd(II). Langmuir isotherm model estimated the adsorption capacities of Fe-Zn-Al LDO adsorbent for As(III), Cd(II) and Pb(II) to be 233 mg/g, 204 mg/g and 256 mg/g, respectively. Fe-Zn-Al LDO adsorbent proved promising for removing As(III), Cd(II) and Pb(II) from surface water and groundwater collected in villages of the Eastern Cape in South Africa.

Acknowledgements The authors wish to acknowledge and thank the University of Johannesburg, Faculty of Science, and Department of Chemical Sciences for laboratory space.

Authors contributions Ramatsobane Rosy Phogole: Conceptualization, Formal analysis, Investigation, Methodology, Validation, Visualization, Writing – original draft. Philani Perfect Mpungose: Conceptualization, Supervision, Visualization, Methodology, Investigation, Validation, Writing – review & editing. Luthando Nyaba: Conceptualization, Supervision, Visualization, Methodology, Investigation, Validation, Writing – review & editing. Mthokozisi Mnguni: Conceptualization, Supervision, Visualization, Methodology, Investigation, Validation, Writing – review & editing. Philiswa Nosizo Nomngongo: Conceptualization, Funding acquisition, Methodology, Project administration, Resources, Software, Supervision, Validation, Visualization, Writing – review & editing.

Funding Open access funding provided by University of Johannesburg. This study was financially supported by the Department of Science and Innovation-National Research Foundation South African Research Chair Initiative (DSI-NRF SARChI) funding instrument, grant no. 91230, National Nanoscience Postgraduate Teaching and Training Platform (NNPTTP) and Water Research Commission (WRC), grant no. C2023-2024–01448.

Data availability Data will be made available upon request.

Declarations

Competing interest The authors declare that they have no known competing financial interests or personal links that could influence the work reported in this work.

References

1. P. Verlicchi, V. Grillini, Surface water and groundwater quality in South Africa and Mozambique—analysis of the most critical pollutants for drinking purposes and challenges in water treatment selection. Water **12**(1), 305 (2020). https://doi.org/10.3390/w12010305
2. S. Matimolane, L. Selane, F.I. Mathivha, Exploring water supply challenges to selected villages of greater Giyani municipality in Limpopo province, South Africa. J. Asian Afr. Stud. 00219096241303946 (2024).
3. A. Apraku, B.A. Gyampoh, J.F. Morton, A.B. Karikari, Water security in rural Eastern Cape, SA: interrogating the impacts of politics and climate change. Sci. Afr. **19**, e01493 (2023). https://doi.org/10.1016/j.sciaf.2022.e01493
4. W.Z. Mandindi, L. Nyaba, N. Mketo, P.N. Nomngongo, Seasonal variation of drinking water quality and human health risk assessment: a case study in rural village of the Eastern Cape. South Africa. Water **14**(13), 2013 (2022). https://doi.org/10.3390/w14132013
5. I.Y. El-Sherif, Polymeric nanofibers for the removal of Cr^{3+} from tannery wastewater. J. Environ. Manag. **129**, 410–413 (2013). https://doi.org/10.1016/j.jenvman.2013.08.004
6. Y. Zou, X. Wang, A. Khan, P. Wang, Y. Liu, A. Alsaedi, T. Hayat, X. Wang, Environmental remediation and application of nanoscale zero-valent iron and its composites for the removal of heavy metal ions: a review. Environ. Sci. Technol. **50**, 7290–7304 (2016). https://doi.org/10.1021/acs.est.6b01897
7. T. Hou, L. Yan, J. Li, Y. Yang, L. Shan, X. Meng, X. Li, Y. Zhao, Adsorption performance and mechanistic study of heavy metals by facile synthesized magnetic layered double oxide/carbon composite from spent adsorbent. Chem. Eng. J. **384**, 123331 (2020). https://doi.org/10.1016/j.cej.2019.123331
8. F. Zhu, X. Tan, W. Zhao, L. Feng, S. He, L. Wei, L. Yang, K. Wang, Q. Zhao, Efficiency assessment of ZVI-based media as fillers in permeable reactive barrier for multiple heavy metal-contaminated groundwater remediation. J. Hazard. Mater. **424**, 127605 (2022). https://doi.org/10.1016/j.jhazmat.2021.127605
9. M.V. Kumar, H.P. Raju, Heavy metals in the environment: sources, fate, and health implications, in *Groundwater resource management planning strategies: a geospatial approach: volume 1*. (Springer Nature Switzerland, Cham, 2025), pp.135–153
10. H. Jiang, Z. Yi, Y. Chen, Y. Li, M. Zhao, J. Wang, Y. Liu, X. Jia, M. Luo, Y. Nie, N. Chi, Innovative application of recyclable magnetic LDO beads for enhancing the remediation of Cd and Pb contamination and the humification during composting. J. Hazard. Mater. **495**, 138863 (2025). https://doi.org/10.1016/j.jhazmat.2025.138863
11. M. Hassan, M.F. Khan, M.S. Mahmud, A. Samad, Potential factors affecting watershed deterioration: a critical review. Water Air Soil Pollut. **236**(9), 607 (2025). https://doi.org/10.1007/s11270-025-08260-z
12. V. Srivastava, P.K. Jha, A. Kumar, Heavy metal pollution assessment of groundwater and associated health risks around the coal mining area, Singrauli, Madhya Pradesh, India. Environ. Monit. Assess. **197**(8), 965 (2025). https://doi.org/10.1007/s10661-025-14398-4
13. A. Karim, Z. Raji, A. Karam, S. Khalloufi, Valorisation of fibrous plant-based food waste as biosorbents for remediation of heavy metals from wastewater-a review. Molecules **28**, 4205 (2023). https://doi.org/10.3390/molecules28104205
14. X. Yang, Y. Wan, Y. Zheng, F. He, Z. Yu, J. Huang, B. Gao, Surface functional groups of carbon-based adsorbents and their roles in the removal of heavy metals from aqueous solutions: a critical review. Chem. Eng. J. **366**, 608–621 (2019). https://doi.org/10.1016/j.cej.2019.02.119
15. A.M.P. Madhubashani, D.A. Giannakoudakis, B. Amarasinghe, A.U. Rajapaksha, P.T.P. Kumara, K.S. Triantafyllidis, M. Vithanage, Propensity and appraisal of biochar performance in removal of oil spills: a comprehensive review. Environ. Pollut. **288**, 117676 (2021). https://doi.org/10.1016/j.envpol.2021.117676
16. H. Chauhan, R. Kumar, R. Gupta, Green synthesis of Zinc oxide (ZnO) nanoparticles from *Allium cepa* (onion) peels for sustainable Cr(VI) removal: adsorption isotherms, kinetics, thermodynamics, and reusability. Water Air Soil Pollut. **236**, 645 (2025). https://doi.org/10.1007/s11270-025-08295-2
17. L.M. Ofiera, P. Bose, C. Kazner, Removal of heavy metals and bulk organics towards application in modified constructed wetlands using activated carbon and zeolites. Water **16**(3), 511 (2024). https://doi.org/10.3390/w16030511
18. Y.G. Wibowo, H. Safitri, Kusumawati et al., Biochar MMT ZnAl LDH composite materials derived from solid waste for heavy metal removal in artificial acid mine drainage. Sci. Rep. **15**, 14914 (2025). https://doi.org/10.1038/s41598-025-96987-4
19. A.K.A. Khalil, I.W. Almanassra, A. Chatla, I. Ihsanullah, T. Laoui, M.A. Atieh, Insights into the adsorption of lead ions by Mg-Al LDH doped activated carbon composites: implications for fixed bed column and batch applications. Chem. Eng. J. **218**, 119192 (2023). https://doi.org/10.1016/j.ces.2023.119192
20. A. Jawad, Z. Liao, Z. Zhou, A. Khan, T. Wang, J. Ifthikar, Z. Chen, Fe-MoS_4: an effective and stable LDH-based adsorbent for selective removal of heavy metals. ACS appl. Mater. Interfaces **9**, 28451–28463 (2017). https://doi.org/10.1021/acsami.7b07208
21. W. Mo, C. He, Y. Yang, B. Cheng, J. Yang, Y. Huang, Adsorption behavior of Mg-Al layered double hydroxide on Pb^{2+}, Zn^{2+}, Cd^{2+}, and As^{5+} coexisting in aqueous solution. Mater. Today Sustain. 100861 (2024). https://doi.org/10.1016/j.mtsust.2024.100861
22. M.M. Savić, M. Vuksanović, N. Savić, A. Knežević, S. Šaponjić, A. Ilić, Egelja, modified silica particles coated with Cu-Al layered double hydroxide for phosphate and arsenate removal in water treatment. Molecules **30**, 2138 (2025). https://doi.org/10.3390/molecules30102138
23. N. Chubar, M. Szlachta, Static and dynamic adsorptive removal of selenite and selenate by alkoxide-free sol–gel-generated Mg–Al–CO_3 layered double hydroxide: effect of competing ions. Chem. Eng. J. **279**, 885–896 (2015). https://doi.org/10.1016/j.cej.2015.05.070
24. Y. Yang, X. Tan, E. Almatrafi, S. Ye, B. Song, Q. Chen, H. Yang, Q. Fu, Y. Deng, Z. Zeng, G. Zeng, Alfalfa biochar supported Mg-Fe layered double hydroxide as filter media to remove trace metal(loid)s from stormwater. Sci. Total. Environ. **844**, 156835 (2022). https://doi.org/10.1016/J.SCITOTENV.2022.156835
25. Y. Hong, J. Peng, X. Zhao, Y. Yan, B. Lai, G. Yao, Efficient degradation of atrazine by CoMgAl layered double oxides catalysed peroxymonosulfate: optimisation, degradation pathways and mechanism. Chem. Eng. J. **370**, 354–363 (2019). https://doi.org/10.1016/j.cej.2019.03.127
26. Y. Li, Z. Xia, T. Zhan, M. Mao, N. Ma, W. Dai, Levofloxacin synergistic capture using a "Memory-Effect" layered double oxides loaded with ZIF-67 nanoparticles. Langmuir **41**(19), 12140–12149 (2025). https://doi.org/10.1021/acs.langmuir.5c00870
27. Y. Huang, C. Liu, S. Rad, H. He, L. Qin, A comprehensive review of layered double hydroxide-based carbon composites as an environmental multifunctional material for wastewater treatment. Processes **10**, 617 (2022). https://doi.org/10.3390/pr10040617
28. W. Yao, S. Yu, J. Wang, Y. Zou, S. Lu, Y. Ai, X. Wang, Enhanced removal of methyl orange on calcined glycerol-modified

nanocrystallined Mg/Al layered double hydroxides. Chem. Eng. J. **307**, 476–486 (2017). https://doi.org/10.1016/j.cej.2016.08.117
29. B. Yang, S. Wei, K. Tang, X. Zhai, Study on the degradation performance of 2, 4-DCP by modified Co–Ni–Fe hydrotalcite. Catal. Lett. **152**, 383–397 (2022). https://doi.org/10.1007/s10562-021-03615-7
30. P. Zhang, L. Zhang, Z. Ke, M. Xiang, Y. Cai, W. Wang, Z. Zhu, Sulfate-loaded layered double oxide: a bifunctional adsorbent for simultaneous purification of metal ion and anionic dye. Appl. Clay Sci. **216**, 106366 (2022). https://doi.org/10.1016/j.clay.2021.106366
31. Y. Kamimoto, N. Okamoto, T. Hagio, J. Yong-Jun, P. Deevanhxay, R. Ichino, Development of magnesium–iron layered double hydroxide and application to nitrate removal. SN Appl. Sci. **1**, 1399 (2019). https://doi.org/10.1007/s42452-019-1240-7
32. F.L. Theiss, G.A. Ayoko, R.L. Frost, Synthesis of layered double hydroxides containing Mg2+, Zn2+, Ca2+ and Al3+ layer cations by co-precipitation methods-a review. Appl. Surf. Sci. **383**, 200–213 (2016). https://doi.org/10.1016/j.apsusc.2016.04.150
33. C. Chen, M. Greenwood, J.C. Buffet, D. O'Hare, Aqueous miscible organic layered double hydroxides as catalyst precursors for biodiesel synthesis. Green Chem. **22**, 3117–3121 (2020). https://doi.org/10.1039/D0GC00571A
34. C. Zhang, J.V. García-Meza, Y. Li, Differential removal of tetracycline hydrochloride and quinolone antibiotics by calcined and uncalcined layered double hydroxides. Miner. Miner. Mater. **2**, 3 (2023). https://doi.org/10.20517/mmm.2022.10
35. D. Sharma, S. Kumar, M. Shandilya, S. Punil, Synthesis and analysis of Ag doped $ZnFe_2O_4$ nanoparticles growth using *Urtica dioica* natura extract. J. Clust. Sci. **35**, 961–973 (2024). https://doi.org/10.1007/s10876-023-02521-9
36. M. Thommes, K. Kaneko, A.V. Neimark, J.P. Olivier, F. Rodriguez-Reinoso, J. Rouquerol, K.S. Sing, Physisorption of gases, with special reference to the evaluation of surface area and pore size distribution (IUPAC technical report). Pure Appl. Chem. **87**, 1051–1069 (2015). https://doi.org/10.1515/pac-2014-1117
37. P. Zhang, W. Wang, W. Liu, P. Li, Y. Cai, J. Chen, N. Ding, Insight into different removal behaviors and mechanism of heavy metals via sulfate-loaded layered double oxide. J. Environ. Chem. Eng. **10**(3), 107751 (2022). https://doi.org/10.1016/j.jece.2022.107751
38. Z. Khoshraftar, A. Ghaemi, A. Hemmati, Comprehensive investigation of isotherm, RSM, and ANN modeling of CO_2 capture by multi-walled carbon nanotube. Sci. Rep. **14**(1), 5130 (2024). https://doi.org/10.1038/s41598-024-55836-6
39. I. Takanashi, T. Kameda, S. Kumagai, Y. Saito, Y. Nomura, D. Kawamura, T. Yoshioka, Synthesis of an Mg–Fe–Al layered double oxide with a high arsenic anion adsorption capacity and the establishment of an arsenic anion desorption process. J. Phys. Chem. Solids **190**, 112017 (2024). https://doi.org/10.1016/j.jpcs.2024.112017
40. J. Hu, W. Xi, Y. Zhang, R. Wang, H. Wang, Y. Gong, B. He, J. Jin, Rational design of LDH-Derived NiFe layered double oxides as capacitive deionization anode for efficient chlorine ion storage with a "memory effect." Appl. Surf. Sci. **687**, 162289 (2025). https://doi.org/10.1016/j.apsusc.2025.162289
41. M. Han, X. Shen, J. Guo, Y. Liu, Y. Zhai, Green synthesis pathway: transforming industrial waste into high-performance MgAl-LDO adsorbent and the innovative applications in heavy metal ions capture. J. Water Process Eng. **73**, 107704 (2025). https://doi.org/10.1016/j.jwpe.2025.107704
42. G.P. Mashile, A. Mpupa, A. Nqombolo, K.M. Dimpe, P.N. Nomngongo, Recyclable magnetic waste tyre activated carbon-chitosan composite as an effective adsorbent rapid and simultaneous removal of methylparaben and propylparaben from aqueous solution and wastewater. J. Water Process Eng. **33**, 101011 (2020). https://doi.org/10.1016/j.jwpe.2019.101011
43. X. Chen, M.F. Hossain, C. Duan, J. Lu, Y.F. Tsang, M.S. Islam, Y. Zhou, Isotherm models for adsorption of heavy metals from water-a review. Chemosphere **307**, 135545 (2022). https://doi.org/10.1016/j.chemosphere.2022.135545
44. J. Febrianto, A.N. Kosasih, J. Sunarso, Y.H. Ju, N. Indraswati, S. Ismadji, Equilibrium and kinetic studies in adsorption of heavy metals using biosorbent: a summary of recent studies. J. Hazard. Mater. **162**(2–3), 616–645 (2009). https://doi.org/10.1016/j.jhazmat.2008.06.042
45. R. Mohrazi, A. Ghasemi-Fasaei, S. Mojiri, Safarzadeh Shirazi, optimisation of LDO-pectin synthesis conditions for the removal of metals from wastewater: a comparison of response surface methods and taguchi approaches. Polymers **15**(18), 3778 (2023). https://doi.org/10.3390/polym15183778
46. W. Lin, J. Zhou, S. Sun, Cadmium and lead removal by Mg/Fe bimetallic oxide-loaded sludge-derived biochar: batch adsorption, kinetics, and mechanism. Environ. Sci. Pollut. Res. **30**(37), 86866–86878 (2023). https://doi.org/10.1007/s11356-023-28574-x
47. P. Zhang, M. Xiang, T. He, H. Liu, S. Yu, X. Pan, Y. Chen, High-efficiency water purification for methyl orange and lead (II) by eco-friendly magnetic sulfur-doped graphene-like carbon-supported layered double oxide. J. Hazard. Mater. **419**, 126406 (2021). https://doi.org/10.1016/j.jhazmat.2021.126406
48. Z.H. Momin, L.P. Lingamdinne, R. Kulkarni, C.A. Pal, Y.L. Choi, Y.Y. Chang, J.R. Koduru, Exploring recyclable alginate-enhanced GCN-LDO sponge for U (VI) and Cd (II) removal: insights from batch and column studies. J. Hazard. Mater. **469**, 134015 (2024). https://doi.org/10.1016/j.jhazmat.2024.134015
49. Y. Huang, X. Luo, C. Liu, S. You, S. Rad, L. Qin, Effective adsorption of Pb (II) from wastewater using MnO_2 loaded MgFe-LD(H)O composites: adsorption behavior and mechanism. RSC Adv. **13**(28), 19288–19300 (2023). https://doi.org/10.1039/d3ra03035k
50. Abushawish, A. Chatla, I.W. Almanassra, A. Shanableh, M.A. Atieh, Co-Al layered double oxide activated carbon composite for eliminating lead ions from water. J. Phys.: Conf. Ser. **2751**(1), 012008 (2024). IOP Publishing. https://iopscience.iop.org/article/10.1088/1742-6596/2751/1/012008/meta
51. Y. Sun, W. Yin, Y. Wang, N.D. Zhao, X.Y. Wang, J.G. Zhang, Q.J. Pan, Fabrication of ultra-thin MgAl layered double oxide by cellulose templating and its immobilisation effect toward heavy metal ions: cation-exchange and deposition mechanism. Chem. Eng. J. **427**, 132017 (2022). https://doi.org/10.1016/j.cej.2021.132017
52. X. Wang, J. Zhu, W. Liu, W. Li, H. Wang, Efficiency and synergy of MnO_2@ LDO for arsenic and fluoride simultaneous sorption from water. AIP Adv. **14**(3) (2024). https://doi.org/10.1063/5.0191593
53. P. Zhang, Y. Cai, L. Zhang, Y. Mao, M. Xiang, Z. Zhu, Y. Zou, Superior selective removal of lead via sulfate doped flower like layered double oxide: an example of high value-added utilisation of organic waste. J. Clean. Prod. **307**, 127267 (2021). https://doi.org/10.1016/j.jclepro.2021.127267
54. I. Takanashi, T. Kameda, S. Kumagai, Y. Saito, Y. Nomura, D. Kawamura, T. Yoshioka, Synthesis of layered double oxide with high specific surface area by innovative sol-gel method through its application to arsenate anion adsorption. J. Alloys Compd. **960**, 170865 (2023). https://doi.org/10.1016/j.jallcom.2023.170865
55. M. Xie, X. Luo, C. Liu, S. You, S. Rad, H. He, Z. Tu, Enhancing mechanism of arsenic (iii) adsorption by MnO_2-loaded calcined MgFe layered double hydroxide. RSC Adv. **12**(40), 25833–25843 (2022). https://doi.org/10.1039/d2ra04805a
56. F. Batool, J. Akbar, S. Iqbal, S. Noreen, S.N.A. Bukhari, Study of isothermal, kinetic, and thermodynamic parameters for adsorption

of cadmium: an overview of linear and nonlinear approach and error analysis. Bioinorg. Chem. Appl. **2018**, 3463724 (2018). https://doi.org/10.1155/2018/3463724

57. N. You, X.F. Wang, J.Y. Li, H.T. Fan, H. Shen, Q. Zhang, Synergistic removal of arsanilic acid using adsorption and magnetic separation technique based on Fe3O4@ graphene nanocomposite. J. Ind. Eng. Chem. **70**, 346–354 (2019). https://doi.org/10.1016/j.jiec.2018.10.035
58. S. Mpelane, A. Mpupa, M. Mlambo, N. Bingwa, N. Mketo, P.N. Nomngongo, Magnetic zeolite@ β-cyclodextrin-gum Arabic nanocomposite for adsorptive removal of levofloxacin. J. Hazard. Mater. Adv. **11**, 100354 (2023). https://doi.org/10.1016/j.hazadv.2023.100354
59. J. Liu, P. Wu, S. Li, M. Chen, W. Cai, D. Zou, N. Zhu, Z. Dang, Synergistic deep removal of As(III) and Cd(II) by a calcined multifunctional MgZnFe-CO_3 layered double hydroxide: photooxidation, precipitation and adsorption. Chemosphere **225**, 115–125 (2019). https://doi.org/10.1016/J.CHEMOSPHERE.2019.03.009
60. G.Y. Abo El-Reesh, A.A. Farghali, M. Taha, M. et al., Novel synthesis of Ni/Fe layered double hydroxides using urea and glycerol and their enhanced adsorption behaviour for Cr(VI) removal. Sci Rep. **10**, 587 (2020). https://doi.org/10.1038/s41598-020-57519-4
61. L. Lu, Z. Wu, J. Bi, H. Zhang, A. Shahab, Calcined MgFe layered double hydroxides for magnetic separation and enhanced adsorption performance of methyl orange: mechanism based on the memory effect. J. Water Process Eng. **63**, 105418 (2024). https://doi.org/10.1016/j.jwpe.2024.105418